Check for updates

Green-light induced cycloadditions†

Philipp W. Kamm,[abc] James P. Blinco, [ID] *[ab] Andreas-Neil Unterreiner [ID] *[c] and Christopher Barner-Kowollik [ID] *[ab]

We introduce a red-shifted tetrazole that is able to undergo efficient nitrile imine-mediated tetrazole–ene cycloaddition (NITEC) under blue and green light irradiation. We provide a detailed wavelength-dependent reactivity map, and employ a number of LEDs for high-conversion small molecule and polymer end-group modification.

Light induced reactions have found widespread use in both industrial and biomedical applications, as well as fundamental research due to their spatio-temporal control and non-invasive nature.[1–4] An even higher level of control can be achieved by tuning the wavelength and intensity of the incident light source. Through activation of different photoactive moieties independently and in a sequential fashion, multicomponent, photo-induced reaction systems have been used to establish λ-orthogonality as a versatile pathway for even more complex reaction routes.[5–10] However, to date, the majority of photo-reactions are triggered with UV light, which is associated with severe limitations such as decreased penetration depth, harmfulness to biological tissue and propensity for side reactions.[11,12] Identifying and developing chromophore moieties that can be activated by visible light and react in an efficient and specific manner therefore is a continuing pursuit. Several strategies have been developed to fulfil these challenging requirements, *i.e.* extending the conjugated system, introducing electron-donating substituents to lower the HOMO–LUMO gap, or non-linear two-photon-absorption processes.[13–15]

Whereas traditionally absorption spectra are used to determine the most efficient irradiation wavelength, our group recently reported that the wavelength-dependent reactivity maximum is often significantly red-shifted compared to the absorption maximum.[16,17] To monitor wavelength-dependent reactivity, we developed the action plot concept, where a wavelength-tuneable ns-laser setup is used as a monochromatic light source to trigger a photo-induced reaction at specific wavelengths, with the laser energy adjusted so that a constant photon count at each wavelength is ensured. Subsequently, the reaction conversion is plotted *versus* the wavelength. Such precise reactivity maps are imperative to install truly λ-orthogonal reaction systems, which – once established – can be conducted using readily available LED setups with a broader (but still controlled) spectral range.[18]

A very promising and widely used UV and visible light addressable reaction is the nitrile imine-mediated tetrazole–ene cycloaddition (NITEC), whereby a 2,5 substituted tetrazole – upon light irradiation – eliminates N_2, forming a highly reactive nitrile imine that can undergo a rapid 1,3-dipolar cycloaddition.[1] First described by Huisgen and Sustmann,[19] it has since been employed for a variety of applications, including protein labelling,[20] nucleic acid modification,[21] polymer ligation,[22] hydrogel assembly,[23] and modification of nanoparticles and microspheres.[24,25] In recent years, researchers have worked on extending the absorption profile of these compounds from UVB into the visible light regime, mostly by introducing substituents or extended conjugated chromophores at the *N*-phenyl ring.[22,26,27] However, to our knowledge, no NITEC reaction so far has been carried out with wavelengths longer than 420 nm in a one photon process.

Herein, we report the synthesis and photoreactivity of a blue to green light activated tetrazole equipped with a dimethylaminopyrenyl moiety (Scheme 1). The wavelength-dependent reactivity is carefully assessed for an exemplary small-molecule ligation reaction, and clean and high-conversion NITEC photoreactions are reported for a number of dipolarophiles, including an end-group functionalized poly(methyl)methacrylate based polymer chain at wavelengths up to 515 nm.

a Centre for Materials Science, Queensland University of Technology (QUT), 2 George Street, Brisbane, QLD 4000, Australia. E-mail: j.blinco@qut.edu.au, christopher.barnerkowollik@qut.edu.au

b School of Chemistry and Physics, Queensland University of Technology (QUT), 2 George Street, Brisbane, QLD 4000, Australia

c Molecular Physical Chemistry Group, Institute of Physical Chemistry, Karlsruhe Institute of Technology (KIT), Fritz-Haber-Weg 2, Geb. 30.44, Karlsruhe 76131, Germany. E-mail: andreas.unterreiner@kit.edu

† Electronic supplementary information (ESI) available. See DOI: 10.1039/d1cc00340b
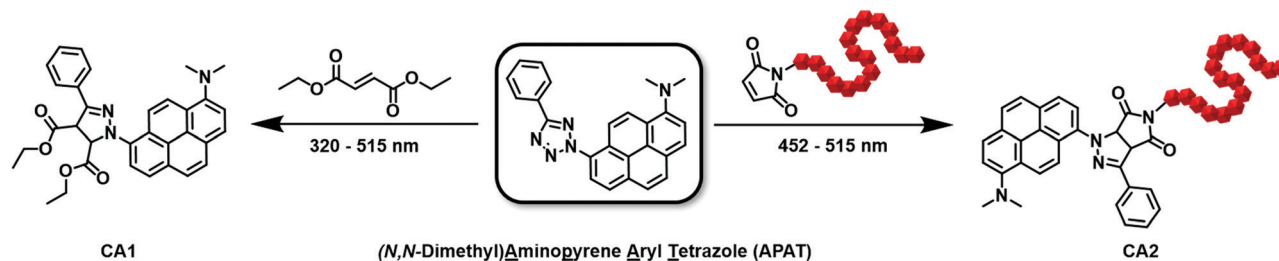
Scheme 1 Synthetic routes for photo-induced NITEC reactions of **APAT**: Left arrow: Small molecule model reaction between **APAT** and diethylfumarate, using a tuneable ns-pulsed laser system in a wavelength range between 320 nm and 515 nm, to precisely monitor the wavelength dependent reactivity. Right arrow: Polymer end-group modification, using three different LEDs, centred around 452 nm, 500 nm, and 515 nm, respectively.

To achieve red-shifted reactivity, it is vital to add extended conjugated systems or electron donating substituents in the N^2 position.[26] Adding a Me$_2$N-group in the *para* position of the N^2-phenylring of a diaryltetrazole shifted the absorption maximum from 302 nm to 336 nm. Similarly, by substituting the N^2 phenyl ring with a pyrene moiety, absorption was shifted to 343 nm.[26,28] We hypothesize that a combination of both strategies allows for an even more red-shifted photoactive molecule, hence, dimethylamino pyrenyl aryl tetrazole (**APAT**) was synthesized in four steps from pyrene-1-amine (Scheme S1, ESI†). This presents a modification of pyrene aryl tetrazole (PAT), which was introduced by our group previously.[22] While introducing a second substituent on the pyrene ring through nitration naturally leads to formation of regio-isomers, only the 1,8-disubstituted species could be isolated in sufficient quantities after chromatography (Scheme 1). The positions of the substituents were confirmed *via* 2D ^{1}H- and ^{13}C-NMR spectroscopy (Fig. S1, ESI†).

Investigation of the absorption properties of **APAT** in MeCN revealed two overlapping broad absorption bands in the long wavelength regime, showing two absorption maxima at 376 nm and 402 nm, which we attributed to transitions into low-lying electronically excited singlet states and to a charge-transfer state, respectively (Fig. 1b, left *y*-axis).[28,29] However, absorbance can be observed up to 500 nm and a slight tailing occurs even well beyond 500 nm (up to 600 nm). Furthermore, two absorption maxima appear in the short wavelength region (237 nm and 291 nm), which can be attributed to transitions into higher excited states. We found a fluorescence quantum yield of 0.39 in MeCN, with emission peaking at 533 nm, leaving a significant portion of absorbed photons potentially available to induce photoreaction (for full absorption and emission spectrum refer to Fig. S2, ESI†).

To investigate the photoreactivity at various wavelengths, small molecule model reactions were conducted in the wavelength range between 320 nm and 525 nm and analysed *via* coupled liquid chromatography and high-resolution mass spectrometry (LC–MS). Gradient-free MeCN was used as the mobile phase, which allowed us to quantify **APAT** and the cycloadduct by correlating the chromatogram peaks with the respective $\varepsilon_{392\,nm}$ in MeCN, where 392 nm is the scanning wavelength of the UV detector. Furthermore, using diethylfumarate as a dipolarophile proved to provide the best separation of **APAT** and cycloadduct **CA1** on the column, hence minimising peak overlap
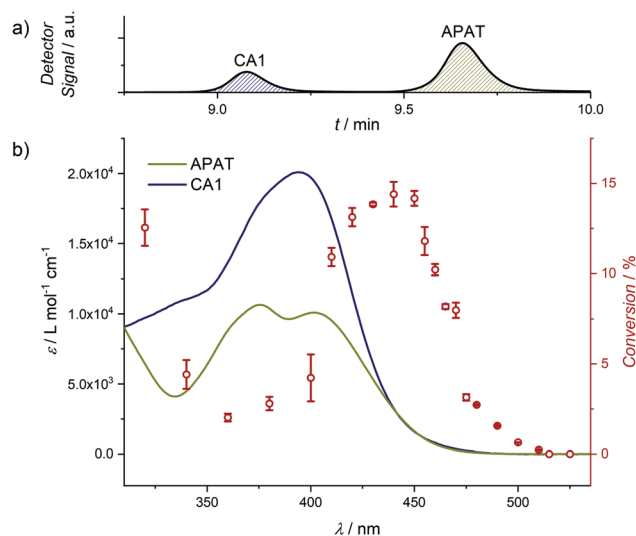
Fig. 1 (a) Exemplary LC chromatogram (scan wavelength: 392 nm) after photoreaction at 440 nm, showing the integrated peaks of **APAT** and **CA1**. (b) Overlay of the absorption profiles of **APAT** (460 μM) and **CA1** (40 μM) (left *y*-axis) and the wavelength-dependent reactivity profile of the photo-induced NITEC reaction between **APAT** and diethylfumarate (right *y*-axis). All experiments were conducted in MeCN and repeated two or three times to obtain error bars. For a detailed description of the laser setup, data processing and conditions of all action plot experiments refer to the ESI.†

(for chromatograms of all tested small molecules, refer to Fig. S4, ESI†), as well as fast conversion. Importantly, the photoreaction proceeded with high selectivity and without significant amounts of side products (at wavelengths 340 nm and lower, degradation of the phenyl tetrazole moiety was observed, yielding dimethylamino pyrene). Critically, unlike previous literature observations, no cycloaddition between the nitrile imine and the solvent, MeCN, was observed.[30] The relative amounts of **CA1** and unreacted **APAT** allowed to calculate the reaction conversion. Since diethylfumarate is a symmetric molecule, it does not lead to different regio-isomers after cycloaddition. Even so, two different product species are present in the ^{1}H-NMR spectrum (Fig. 2): the first corresponds to the pyrazoline adduct, which is expressed by two additional signals at $\delta = 5.55$ ppm and 4.84 ppm. The second corresponds to the pyrazole adduct after rearomatization, hence loss of the two aforementioned signals. Photoreactions between **APAT** and diethylfumarate were conducted in a wavelength range
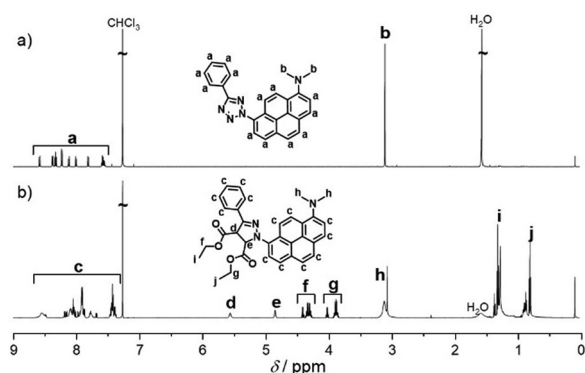
Fig. 2 ^{1}H-NMR spectra before and after NITEC reaction using a 10 W 452 nm LED. Zoomed-in spectra are available in the ESI,† (Fig. S7 and S19). (a) **APAT** before irradiation. (b) Cycloadduct after purification via column chromatography. While in the spectrum both the pyrazoline and the re-aromatized pyrazole species are present, for clarity, only the pyrazoline cycloadduct without specification of the stereo-active centres is depicted.

between 320 nm and 525 nm and used to compile the wavelength-dependent reactivity map. ^{1}H-NMR and absorption spectra of **CA1** were obtained after synthesizing a larger quantity, using a 452 nm centred 10 W LED, which then could be isolated and purified by column chromatography. Interestingly, unlike reported in previous studies on NITEC reactions, **CA1** is non-fluorescent and fluorescence intensity decreases by a factor of 100 during the course of the photoreaction.

The action plot depicted in Fig. 1 reveals that the reactivity map does not follow the absorption spectrum. While an absorption minimum occurs at 335 nm, the reactivity minimum is shifted to 360 nm, yielding 2% conversion. Whereas the absorption spectrum shows two maxima in the investigated wavelength regime, only one broad reactivity band is observed, peaking between 430 nm and 450 nm (14% conversion), which is significantly red-shifted compared to the absorption maximum (402 nm). Since we were mainly interested in the photoreactive behaviour in the visible regime, more data points were recorded at wavelengths between 410 nm and 525 nm. Apart from an outlier at 470 nm, conversion gradually decreases with higher wavelengths. While no conversion was observed at 515 nm and above under the given conditions, significant conversion was achieved when the number of incident photons was increased by a factor of 25 (Fig. S5, ESI†), demonstrating that – while less efficient than with blue light – the reaction can be triggered with green light wavelengths. We refrained from driving the reaction to higher conversions in the wavelength-dependence study, since with higher conversion competing absorption through formation of the cycloadduct is no longer negligible. Nevertheless, we are able to demonstrate that high conversions are possible with a substantially increased number of photons, driving the reaction to 89% conversion with 465 nm irradiation (Fig. S6, ESI†).

With the detailed action plot at hand, we proceeded to employ **APAT** for polymer end-group modification (Scheme 1, right arrow), using a range of different LEDs centred around 452 nm, 500 nm and 515 nm, respectively. To that end, a maleimide functional PMMA based polymer was synthesized via reversible

addition–fragmentation chain-transfer (RAFT) polymerization. Since the ω-terminal dithiocarbonyl group inherently incorporated during this process is strongly coloured and prone to side reactions, it was removed and exchanged for a hydroxy group (Scheme S2, ESI†). To ensure sufficient end-group reactivity (higher for low molecular weights), but also facilitate precipitation after the photoreaction, a medium molecular weight (M_n = 5.2 kDa, $Đ$ = 1.15, refer to ESI,† for the full molecular weight distribution) was chosen for the polymer chains. Four equiv. of **APAT** were irradiated with 1 equiv. of PMMA-Mal in MeCN. Differences in output powers and photon energy of the LEDs were accounted for by adjusting the irradiation time (for detailed description of the setup refer to ESI†). Unreacted **APAT** was separated from **CA2** by using preparative size exclusion chromatography (SEC), and after precipitation **CA2** was analysed by ^{1}H-NMR spectroscopy (Fig. 3 and Fig. S8, ESI†) and size exclusion chromatography (Fig. S10, ESI†). The spectra reveal presence of two different species of **CA2**, corresponding to the pyrazoline cycloadduct and the rearomatized pyrazole cycloadduct. These findings were confirmed by diffusion-ordered spectroscopy (DOSY) and correlation spectroscopy (COSY) (Fig. S8, ESI†). The relative extent to which these two species are formed is difficult to predict and varies in every experiment, which is why both species are treated and quantified as one.

The ^{1}H-NMR spectrum after 452 nm irradiation for 2.5 h (Fig. 3, green line) shows no remaining PMMA-Mal peak (HC=CH) at δ = 6.75 ppm anymore, indicating quantitative end-group conversion. A significant amount of pyrazoline cycloadduct is still present. After 500 nm irradiation for 3.7 h, peak ratios correspond to 50%
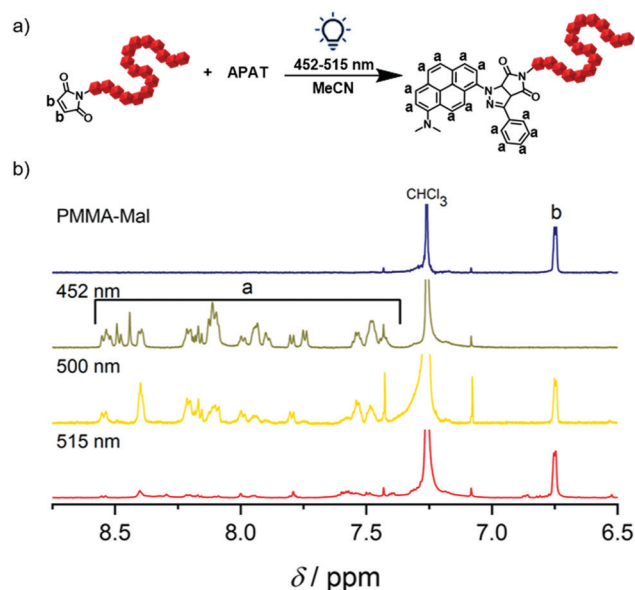

Fig. 3 Polymer end-group modification and analysis. (a) Reaction scheme of the 1,3-dipolar cycloaddition of a maleimide end-capped PMMA polymer and **APAT**, forming the pyrazoline cycloadduct. (b) Zoom into the aromatic region of ^{1}H-NMR spectra of **CA2** after photo-induced polymer end-group modification. Reaction conversion was determined by comparing the resonance integrals of the aromatic protons (a = 13 H) and remaining vinylic protons of the maleimide end-group (b = 2 H). For reference, the spectrum of PMMA-Mal is depicted in blue. Full spectra are available in the ESI.†

conversion (yellow line). Unreacted tetrazole could be recovered as a pure compound after preparative SEC. Critically, when longer irradiation times were applied (2 d irradiation at 500 nm), we were able to drive the reaction to 100% end-group conversion (Fig. S8, ESI†). After 515 nm irradiation for 4.3 h, only traces of **CA2** are detected in the spectrum, but could not be quantified.

These findings show that **APAT** can react with both small molecule and macromolecular dipolarophiles. We also modified **APAT** to bear a linker (**1b**, refer to ESI†) consisting of a hydroxy-functional undecyl chain attached to the C^5-phenyl ring, which can serve as an initiator, hence allowing for polymerization of **APAT** and employing it for polymer–polymer ligation. Interestingly, the novel green light reactive tetrazole may feature pH-responsivity, since the dimethylamino group can act as a base and the absorption spectrum is significantly blue-shifted upon acidification (Fig. S11, ESI†).

In summary, we introduce the design and synthesis of a green light reactive tetrazole by combining two strategies: extending the conjugated system and introducing electron-donating substituents. Without the need for catalysts, the tetrazole reacts cleanly with a variety of dipolarophiles, including a maleimide-functional polymer and diethylfumarate, at wavelengths up to 515 nm, which to date is the most red-shifted wavelength employed to activate a tetrazole in a single-photon process. Critically, we provide a detailed wavelength-dependent reactivity map, revealing a reactivity minimum at 360 nm and a maximum between 430 nm and 450 nm, making this molecule a promising candidate for λ-orthogonal reaction systems. With the detailed reactivity map available, we were able to employ the tetrazole for high-conversion polymer end-group modification, using widely available blue and green LEDs.

Conflicts of interest

There are no conflicts to declare.

Notes and references

1 G. S. Kumar and Q. Lin, *Chem. Rev.*, 2020, DOI: 10.1021/acs.chemrev.0c00799.
2 K. Jung, N. Corrigan, M. Ciftci, J. Xu, S. E. Seo, C. J. Hawker and C. Boyer, *Adv. Mater.*, 2020, **32**, 1903850.
3 C. Brieke, F. Rohrbach, A. Gottschalk, G. Mayer and A. Heckel, *Angew. Chem., Int. Ed.*, 2012, **51**, 8446–8476.
4 M.-M. Russew and S. Hecht, *Adv. Mater.*, 2010, **22**, 3348–3360.
5 M. M. Lerch, M. J. Hansen, W. A. Velema, W. Szymanski and B. L. Feringa, *Nat. Commun.*, 2016, **7**, 12054.
6 H. Frisch, D. E. Marschner, A. S. Goldmann and C. Barner-Kowollik, *Angew. Chem., Int. Ed.*, 2018, **57**, 2036–2045.
7 V. X. Truong, F. Li, F. Ercole and J. S. Forsythe, *ACS Macro Lett.*, 2018, **7**, 464–469.
8 M. J. Hansen, W. A. Velema, M. M. Lerch, W. Szymanski and B. L. Feringa, *Chem. Soc. Rev.*, 2015, **44**, 3358–3377.
9 J. R. Hemmer, S. O. Poelma, N. Treat, Z. A. Page, N. D. Dolinski, Y. J. Diaz, W. Tomlinson, K. D. Clark, J. P. Hooper, C. Hawker and J. Read de Alaniz, *J. Am. Chem. Soc.*, 2016, **138**, 13960–13966.
10 J. P. Olson, M. R. Banghart, B. L. Sabatini and G. C. R. Ellis-Davies, *J. Am. Chem. Soc.*, 2013, **135**, 15948–15954.
11 S. Stolik, J. A. Delgado, A. Pérez and L. Anasagasti, *J. Photochem. Photobiol., B*, 2000, **57**, 90–93.
12 E. Sage, P.-M. Girard and S. Francesconi, *Photochem. Photobiol. Sci.*, 2012, **11**, 74–80.
13 G. M. Tsivgoulis and J. M. Lehn, *Adv. Mater.*, 1997, **9**, 627–630.
14 D. Bléger and S. Hecht, *Angew. Chem., Int. Ed.*, 2015, **54**, 11338–11349.
15 C. P. Ramil and Q. Lin, *Curr. Opin. Chem. Biol.*, 2014, **21**, 89–95.
16 D. E. Fast, A. Lauer, J. P. Menzel, A.-M. Kelterer, G. Gescheidt and C. Barner-Kowollik, *Macromolecules*, 2017, **50**, 1815–1823.
17 D. E. Marschner, P. W. Kamm, H. Frisch, A.-N. Unterreiner and C. Barner-Kowollik, *Chem. Commun.*, 2020, **56**, 14043–14046.
18 H. Frisch, F. R. Bloesser and C. Barner-Kowollik, *Angew. Chem., Int. Ed.*, 2019, **58**, 3604–3609.
19 J. S. Clovis, A. Eckell, R. Huisgen and R. Sustmann, *Chem. Ber.*, 1967, **100**, 60–70.
20 W. Song, Y. Wang, J. Qu, M. M. Madden and Q. Lin, *Angew. Chem., Int. Ed.*, 2008, **47**, 2832–2835.
21 K. Krell, D. Harijan, D. Ganz, L. Doll and H.-A. Wagenknecht, *Bioconjugate Chem.*, 2020, **31**, 990–1011.
22 P. Lederhose, K. N. R. Wüst, C. Barner-Kowollik and J. P. Blinco, *Chem. Commun.*, 2016, **52**, 5928–5931.
23 O. Guaresti, L. Crocker, T. Palomares, A. Alonso-Varona, A. Eceiza, L. Fruk and N. Gabilondo, *J. Mater. Chem. B*, 2020, **8**, 9804–9811.
24 L. Delafresnaye, N. Zaquen, R. P. Kuchel, J. P. Blinco, P. B. Zetterlund and C. Barner-Kowollik, *Adv. Funct. Mater.*, 2018, **28**, 1800342.
25 L. Delafresnaye, J. P. Hooker, C. W. Schmitt, L. Barner and C. Barner-Kowollik, *Macromolecules*, 2020, **53**, 5826–5832.
26 Y. Wang, W. J. Hu, W. Song, R. K. V. Lim and Q. Lin, *Org. Lett.*, 2008, **10**, 3725–3728.
27 P. An, Z. Yu and Q. Lin, *Chem. Commun.*, 2013, **49**, 9920–9922.
28 E. Blasco, Y. Sugawara, P. Lederhose, J. P. Blinco, A.-M. Kelterer and C. Barner-Kowollik, *ChemPhotoChem*, 2017, **1**, 159–163.
29 S. Techert, S. Schmatz, A. Wiessner and H. Staerk, *J. Phys. Chem. A*, 2000, **104**, 5700–5710.
30 Z. Li, L. Qian, L. Li, J. C. Bernhammer, H. V. Huynh, J.-S. Lee and S. Q. Yao, *Angew. Chem., Int. Ed.*, 2016, **55**, 2002–2006.